*metals*

Article

# Microstructure, Texture Evolution, and Mechanical Properties of MDFed GWZ Alloy Containing LPSO Phases on the Condition of High and Low Temperature Cycle Deformation

**Beibei Dong, Zhimin Zhang *, Xin Che, Jianmin Yu, Mu Meng and Jinlu Zhang**

College of Materials Science and Engineering, North University of China, Taiyuan 030051, China; dongbb1111@163.com (B.D.); CXIN19931029@163.com (X.C.); nucmajin@163.com (J.Y.); SZHENGNUC@163.com (M.M.); nucyangfulai@163.com (J.Z.)

* Correspondence: ZZMNUC@163.com; Tel.: +86-351-392-1778

Received: 23 December 2019; Accepted: 14 January 2020; Published: 16 January 2020

**Abstract:** The current work systematically investigated the microstructure, texture evolution, and mechanical properties of MDFed Mg-13Gd-4Y-2Zn-0.5Zr (wt%) alloy (GWZ) on the condition of high and low temperature cycle deformation. The high and low temperature cycle deformation was proposed on the basis of the conventional multi-directional forging (MDF) at decreasing temperature and annealing treatment. As a new method, it was aimed to timely uniform the microstructure and strengthen magnesium (Mg) matrix during the deformation process. A low accumulative strain of 3 after 1 pass resulted in a bimodal microstructure with undynamic recrystallized (unDRXed) regions and dynamic recrystallized (DRXed) grains, while a high accumulative strain of 12 after 4 passes lead to a homogeneous microstructure with fine DRXed grains. According to the experimental results, it indicated that the average grain size of 63 μm after homogenization treatment at 520 was refined remarkably to 5.20 μm after 4 passes at 420 °C through high and low temperature cycle deformation. The area fraction of DRXed grains was increased to 98.4%, which can be regarded as achieving complete DRX after 4 passes. The grain refinement was mainly caused by particle stimulation nucleation (PSN) and mechanism. As the MDF passes and accumulative strain increased, the basal texture was weakened and transformed from a strong basal texture to a random distribution gradually. Compared with conventional MDF at decreasing temperature, the mechanical properties were enhanced effectively. After 4 passes, the ultimate tensile strength (UTS), tensile yield strength (TYS), and failure elongation (FE) were 405 MPa, 305 MPa, and 13.1%, respectively.

**Keywords:** microstructure; texture evolution; mechanical properties; Mg-13Gd-4Y-2Zn-0.5Zr alloy; high and low temperature cycle deformation

## 1. Introduction

As the lightest metallic constructional material, Mg and Mg alloys possess the low density that is approximately 2/3 of that of aluminum and 1/4 that of steel, have attracted the attention of many scholars, and is widely used in industrial applications [1]. Due to their low densities and high specific strengths, Mg and Mg alloys have attracted considerable recent attention [2–4]. However, the application of Mg alloys in the industry is still limited because of their moderate properties, such as the low yield stress and poor workability at room temperature (RT) [5]. Adding rare earth (RE) elements to pure Mg and heat treatment are effective ways to improve the strength of Mg alloys [6–8]. Nowadays, many researches have been focused on wrought Mg-Gd/Y based alloys due to their superior mechanical properties [9–13]. Homma et al. [11] reported a high-strength Mg-10Gd-5.7Y-1.6Zn-0.5Zr alloy exhibiting a TYS of 473 Mpa and elongation (EL) of 8.0% after hot extrusion and aging treatment. It could be concluded that the refined grains and long period stack ordered (LPSO) phases play important roles in improving mechanical properties. Yu et al. [14] showed Mg-11.5Gd-4.5Y-1.5Zn-0.4Zr alloy exhibiting excellent mechanical performance that TYS of 377 ± 1.2 MPa and EL of 10.8% ± 2.0% by pre-annealing for 1 h of an extruded alloy, which attributed to the Mg5RE phases, LPSO phases, solute segregated Schmidt factors (SFs), and the texture. Peng et al. [15] found that the outstanding mechanical properties can be observed about the UTS, YS, and FE of 310 MPa, 280 MPa, and 2.8% at RT after the T6 heat treatment of the Mg-Gd based alloys. The finer microstructure and precipitated phases significantly increased the mechanical properties.

The high mechanical performance can be obtained through refining grains effectively by severe plastic deformation (SPD) methods. As one of the SPD methods, MDF has especially attracted more and more scholars' attention due to its simple operation and low-cost [16,17]. As we all know, the microstructure after multi-passes deformation and large strain is relatively homogeneous, and the heat treatment process can also uniform the deformed alloy to some extent. Meanwhile, Saboori et al. [18] found that stacking fault energy, as one of the influencing factors, determines the softening mechanism of metal materials, so that the DRX mechanism can be occurred at a specific temperature and strain rate. So, the homogeneous microstructure has a great relationship with deformation passes and heat treatment. Yu et al. [14,19,20] investigated that the high extrusion ratio of 30:1 lead to a uniform microstructure with fine DRXed grains, while the low extrusion ratio of 6:1 resulted in a bimodal microstructure with undeformed regions and DRXed grains. The bimodal microstructure can be removed by subsequent annealing treatment. To further get the homogeneous microstructure and improve the mechanical properties of the deformed alloy, the subsequent heat treatment is proposed and applied to each pass of the MDFed alloy. The conventional MDF process is shown in Figure 1a. As we all know that annealing treatment is an efficient method to modify the mechanical behaviors of wrought Mg alloys. The conventional MDF method is only to use the increased deformation passes and the subsequent heat treatment method to uniform the microstructure of the deformed alloy and improve the mechanical properties of the material. To overcome this challenge, on the basis of not increasing the passes of MDF deformation, a new deformation process is proposed shown in Figure 1b and the new processing method is defined as high and low temperature cycle deformation.

In this work, we utilized a homogenzied Mg-13Gd-4Y-2Zn-0.5Zr alloy (denoted as GWZ) containing LPSO phases as the experimental material. The purpose of the investigation is understanding the effects of the high and low temperature cycle deformation on the microstructure, texture, and mechanical properties. In addition, the paper is aimed to provide a new method to timely uniform the MDFed microstructure and improve the mechanical properties of the MDFed alloy.

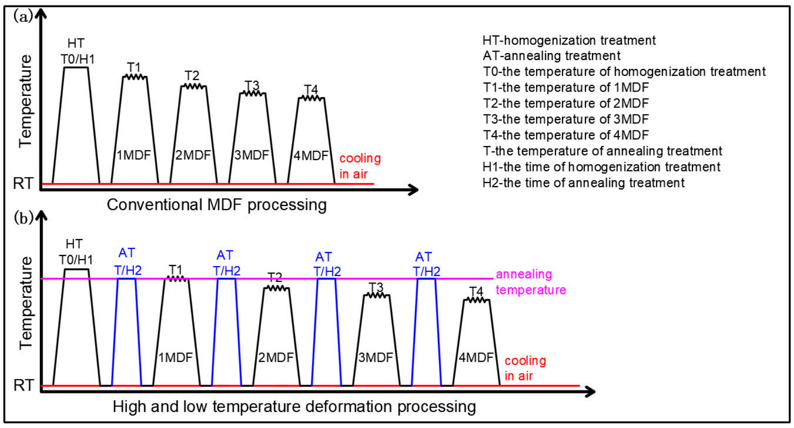


**Figure 1.** The chart of MDF process: (**a**) Conventional method, (**b**) high and low temperature cycle deformation process.

## 2. Materials and Methods

Cylindrical billet of the Mg-13Gd-4Y-2Zn-0.5Zr alloy was produced by semi-continuous casting with 1000 mm in height and 330 mm in diameter provided by Shanxi Wenxi Yinguang Mg Industry Group. Its chemical constituents were listed in Table 1. The Mg-13Gd-4Y-2Zn-0.5Zr cast ingot was homogenized at 520 °C for 16 h followed by air quench. The position of the experimental samples was shown in Figure 2a.

**Table 1.** The chemical constituents of the Mg-13Gd-4Y-2Zn-0.5Zr alloy.

| **Element** | **Gd** | **Y** | **Zn** | **Zr** | **Si** | **Cu** | **Mg** |
|---|---|---|---|---|---|---|---|
| Wt% | 12.88 | 4.00 | 2.00 | 0.50 | <0.01 | <0.01 | Bal. |

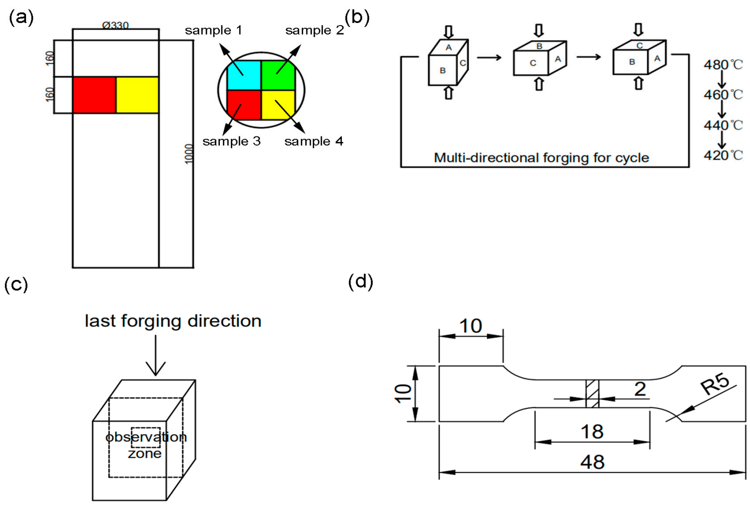


**Figure 2.** (**a**) The position of the experimental samples out of the homogenized rod, (**b**) the schematic representation of geometry changes during each pass of the MDF process, (**c**) microstructure analysis zone for samples after MDF, (**d**) dimensions of tensile samples (in mm).

In the actual production process, a hydraulic press with a 1250 tons limit and the forging speed of 5 mm/s was carried on the MDF process. The four rectangular experimental samples with dimensions of 130 mm × 130 mm × 160 mm were used, and the position of the experimental samples were shown in Figure 2a. The MDF dies and experimental samples were heated to the given temperature. Once the MDF dies and experimental samples attained the desired temperature, a period of 0.5 and 2.5 h were allowed to elapse before subsequent deformation. The schematic representation of the MDF was shown in Figure 2b. In the present work, MDF procedure under constant temperature conditions was composed of the following steps: (1) To study the microstructure and texture evolution, the MDFed alloys after different passes (1,2,3,4) followed by air cooling were denoted as 1MDF, 2MDF, 3MDF, 4MDF, (2) when the 1, 2, 3 passes finished, annealing treatment of 480 °C for 8 h was subjected to the MDFed alloy, then cooled in air, (3) in order to reduce the friction between billets and dies, graphite lubrication was adopted. During the MDF process, for each MDF direction, such as X, Y, Z, the strain is 1. The total true strain of per pass is calculated by the equation:

$$\sum \varepsilon = \frac{\ln H_1}{\ln H_X} + \frac{\ln H_2}{\ln H_Y} + \frac{\ln H_3}{\ln H_Z} \tag{1}$$

where $H_1$, $H_2$, $H_3$ and $H_X$, $H_Y$, $H_Z$ represent the initial and final heights of X, Y, Z direction, respectively.

The forging direction was rotated by 90° step by step (i.e., A to C to B to A to ... ), the three forging steps mentioned above are called a forging pass, as shown in Figure 2b, leading to a cumulative strain of around $\sum\Delta = 3$. Then, the samples were forged by MDF experiments with the cumulative strain of △ = 3 per pass, under the decreasing temperature from 480 to 420 °C by a drop of 20 °C every pass. The experimental parameters are shown in Table 2.

**Table 2.** Designation and history of the studied samples.

| Designation | History |
|---|---|
| Sample 1 | 1st pass MDF at 480 °C ($\sum\Delta\varepsilon = 3$) |
| Sample 2 | 1st pass MDF at 480 °C + annealing treatment at 480 °C + 2nd pass MDF at 460 °C ($\sum\Delta\varepsilon = 6$) |
| Sample 3 | 1st pass MDF at 480 °C + annealing treatment at 480 °C + 2nd pass MDF at 460 °C + annealing treatment at 480 °C + 3rd pass MDF at 440 °C ($\sum\Delta\varepsilon = 9$) |
| Sample 4 | 1st pass MDF at 480 °C +annealing treatment at 480 °C + 2nd pass MDF at 460 °C + annealing treatment at 480 °C + 3rd pass MDF at 440 °C + annealing treatment at 480 °C + 4th pass MDF at 420 °C ($\sum\Delta\varepsilon = 12$) |

The microstructures were observed with optical microscopy (OM) of Zeiss Axio Imager A2m, scanning electron microscopy (SEM) using Hitachi SU5000 (Hitachi, Tokyo, Japan) at 30 kV. As shown in Figure 2c, samples for analysis with the size of 10 mm × 10 mm × 10 mm were carried out in the central part of specimens parallel to the last forging direction. The samples were initially polished by various grades of polishing papers, then mechanically polished with 1.0 μm diamond paste and finally etched in a solution of 1 g picric acid, 2 mL acetic acid, 2 mL distilled water, and 14 mL alcohol for microstructure observation. The initial average grain size of as-homogenized Mg-13Gd-4Y-2Zn-0.5Zr alloy and samples after annealing treatment were measured by using the mean linear intercept method. The grain size distribution in the alloy was analyzed from the microstructure image using Image-Pro Plus Software.

Moreover, the texture evolution was observed by SEM mentioned above equipped with an EDAX/TSL (EDAX Inc., Mahwah, NJ, USA) electron back scattered diffraction (EBSD) operating. To better characterize the results of EBSD, the specimens were polished by using multi-function ion milling with the operating voltage of 6.5 kV and gun angle of 3°. Orientation imaging microscopy (OIM) software (EDAX Inc., Mahwah, NJ, USA) was used to extract EBSD data. Meanwhile, the composition analysis for phases was executed by X-ray diffraction (XRD, Smart Lab SE, Tokyo, Japan) with Cu K$\alpha$ radiation operated at 40 kV and 40 mA, and transmission electron microscopy (TEM) using JEOL JEM-F200 TEM (JEOL, Tokyo, Japan) operating at 200 kV. The average grain size of MDFed alloys were determined by EBSD data and the grains less than 10 μm in diameter were considered to be DRXed grains.

To determine the tensile properties, the samples were machined perpendicular to the last forging direction and dimension of tensile samples was shown in Figure 2d. The tensile tests were carried out by INSTRON 3382 (INSTRON, Norwood, MA, USA) tensile machine at RT and the tensile rate was 1 mm/min.

## 3. Results and Discussion

### *3.1. Microstructural Characterizations*

#### 3.1.1. Microstructure after Homogenization Treatment

Figure 3 shows OM and SEM images of the Mg-13Gd-4Y-2Zn-0.5Zr alloy after homogenization treatment of 520 °C for 16 h. The microstructure after homogenization treatment contains block-shaped LPSO phases at grain boundaries (black arrows) and lamellar-shaped LPSO phases inside grains (yellow arrows). The eutectic phases are Mg5RE (green arrows) by EDS analysis. In addition, a small number of cubiod phases of rare-earth-rich phases (red arrow) also exist. The average grain size is about 63 μm by a mean linear intercept method.

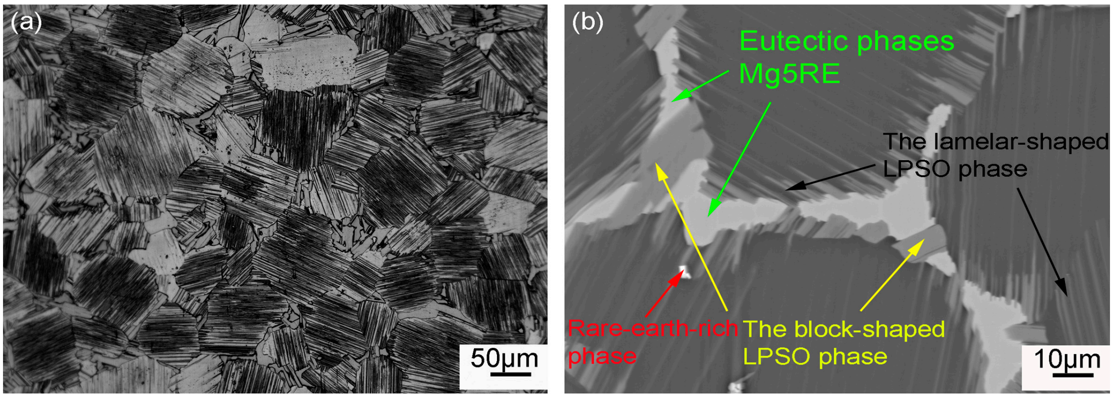


**Figure 3.** Microstructure of the Mg-13Gd-4Y-2Zn-0.5Zr alloy after homogenization treatment: (**a**) OM, (**b**) SEM.

### 3.1.2. Microstructure after High and Low Temperature Cycle Deformation

Figure 4 shows the microstructures of MDFed alloys at 480, 460, 440, 420 °C, respectively. It is clear from Figure 4a,b that DRX occurred after 1 pass at 480 °C, but the grains are nonuniform because of the exist of the undeformed grains. The obtained microstructure can be regarded as a bimodal microstructure that consists of coarse grains and fine grains. The reason for the formation of the bimodal microstructure is that the existence of LPSO phases hinder the movement of dislocations, and by applying more strain, the dislocation density near LPSO phases increases providing the required energy for the nucleation of new grains. As a result, the new grains are evolved along previous coarse-undeformed grains, leading to a bimodal microstructure [21–24]. This deformation mechanism can be seen as PSN. The average grain size is 15.72 μm as shown in Figure 5a. When continued annealing treatment is subjected at 480 °C for 8 h to the 1MDFed sample, followed by air cooling at 25 °C. It can be observed from Figure 6a,d that the microstructure of 1MDFed alloy becomes uniform and can be regarded as equiaxed crystal. This is because there are a large number of sub-boundaries in the 1MDFed alloy. The subgrains reach a stable state by absorbing energy in the annealing process. In addition, a large amount of precipitated phases dissolve into the Mg matrix, and only a small portion of the precipitations exist at the grain boundaries and inside the grains. Figure 4c,d show the microstructure of 2MDFed alloy at 460 °C, it can be found that not only fine particles precipitate at the boundaries, but also plate-like precipitations occur interior of the grains. According to the XRD results shown in Figure 7 and the compositions of Mg81.59Gd12.74Y4.38Zn0.73Zr0.56 and Mg84.43Gd10.66Y3.68Zn0.67Zr0.55 by EDS analysis (red arrows in Figure 4d), the precipitates in different shape all may be Mg5(Gd,Y,Zn). In order to further determine the structure of the precipitated phases, we also perform a TEM experiment, as shown in Figure 8, which demonstrates that the fine particles and the plate-like precipitated phases are Mg5(Gd,Y,Zn). Moreover, the plate-like precipitates are also demonstrated as Mg5RE phase in [14]. However, the average grain size of the 2MDFed sample is 25.83 μm due to the abnormal grain growth, it may be that because of the small volume fraction and weak pinning effect of fine Mg5(Gd,Y,Zn) phases precipitated from the grain boundaries, the grains grow abnormally. At this time, a large amount of plate-like Mg5(Gd,Y,Zn) phases existing in the grain is in an unstable state, because it does not appear in the subsequent process. When annealing treatment of 480 °C and 8 h is conducted to the 2MDFed sample, most of plate-like Mg5(Gd,Y,Zn) precipitations are dissolved into the matrix after annealing treatment, the uniform microstructure can be obtained as shown in Figure 6b,e. When the samples are forged at 440 and 420 °C, the average grain size gradually decreases with the increase of the forging passes. The average grain size of the 3MDFed and 4MDFed sample are 6.52 and 5.20 μm, respectively. In addition, the microstructure of samples become more and more uniform with the increase of forging passes and the decrease of forging temperature, obviously. It can be concluded that the static recrystallization (SRX) mechanism by annealing treatment can be used to obtain a distinct uniform microstructure between the deformation passes.

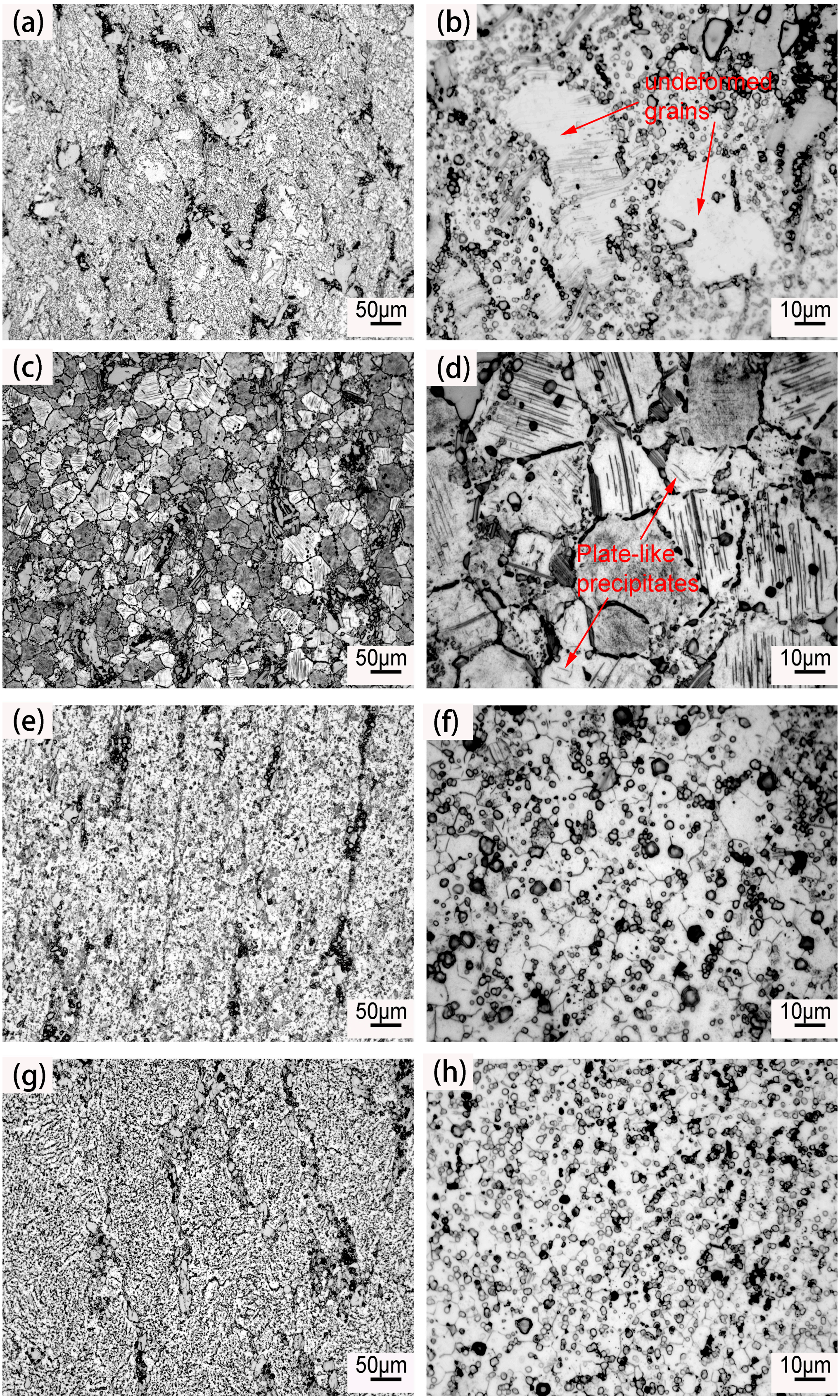


**Figure 4.** The OM images of MDFed alloy after different passes: (**a**,**b**) 1 pass, (**c**,**d**) 2 passes, (**e**,**f**) 3 passes, (**g**,**h**) 4 passes.

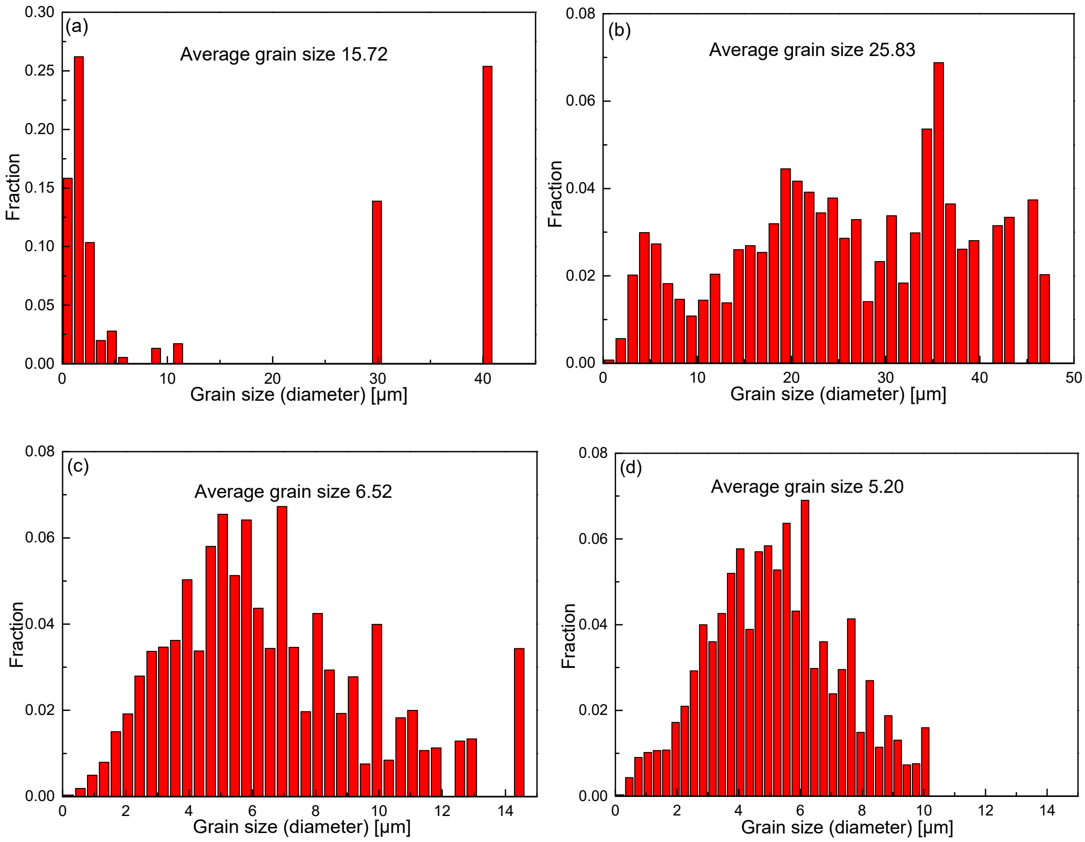


**Figure 5.** The average grain size of MDFed alloy after different passes: (**a**) 1 pass, (**b**) 2 passes, (**c**) 3 passes, (**d**) 4 passes.

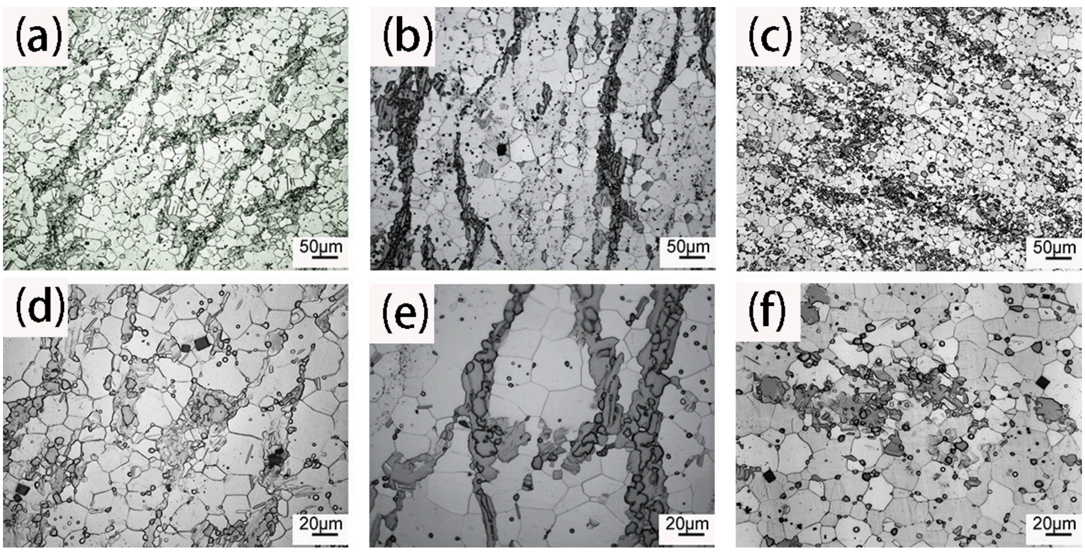


**Figure 6.** The OM images after annealing treatment of 480 °C for 8 h of (**a**,**d**) 1MDFed sample; (**b**,**e**) 2MDFed simple; (**c**,**f**) 3MDFed simple.

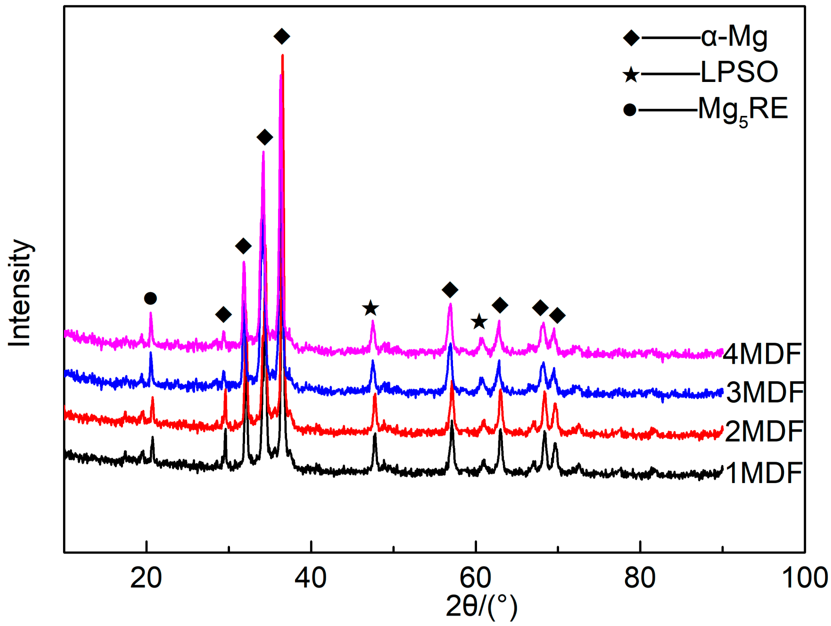


**Figure 7.** X-ray diffraction patterns of MDFed alloy after different passes.

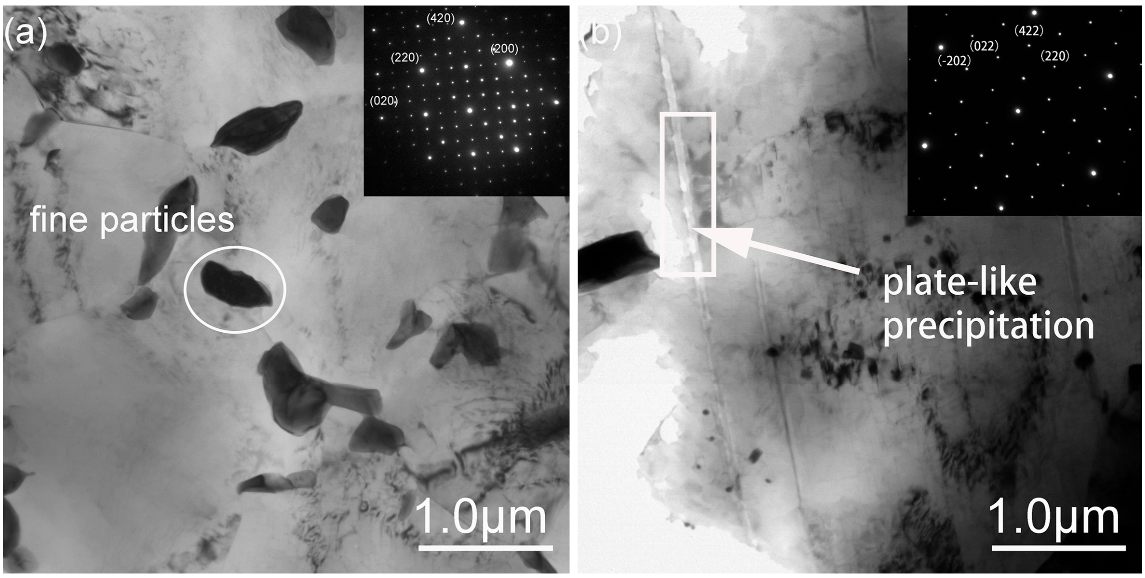


**Figure 8.** The TEM images of fine particles and plate-like precipitation: (**a**) Fine particles, (**b**) plate-like precipitation.

Figure 9 exhibits the trend about volume fraction of DRXed grains, deformed grains, and average grain size after different MDF passes. Combined with the microstructures of the MDFed Mg-13Gd-4Y-2Zn-0.5Zr experimental alloy up to different passes shown in Figure 4, applying the MDF technique has resulted in arrays of fine new grains embedded in the initial grains [25]. The as-homogenized alloy with the mean grain size of 63 μm has been replaced by fine grains of 5.20 μm after 4 passes. It indicates the occurrence of recrystallization mechanism during the high and low temperature cycle deformation. The DRX and SRX mechanism happened in the condition of the MDF process and annealing treatment, respectively. The grain refinement is mainly attributed to the combination of PSN and DRX mechanism [26]. The volume fraction of DRXed grains up to different MDF passes are 59.0%, 12.7%, 87.1%, and 98.4%. Thereby, the average grain size of Mg-13Gd-4Y-2Zn-0.5Zr alloy after different passes is reduced in addition to the 2MDFed alloy. It can be interpreted as the DRXed grains of the 1MDFed alloy have grown abnormally after annealing treatment of 480 °C for 8 h. In addition, the uniform microstructure is mainly caused by SRX mechanism.

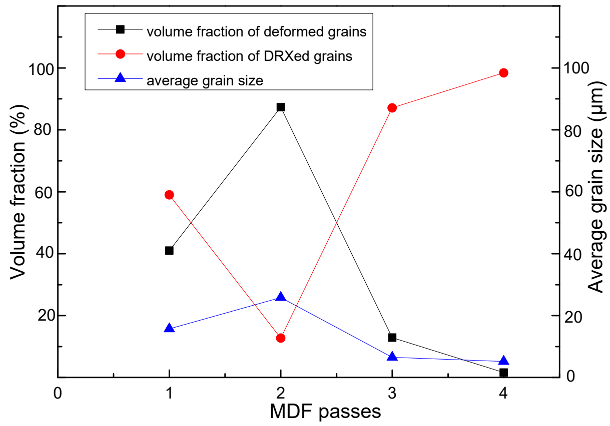


**Figure 9.** The trend about volume fraction of DRXed grains, deformed grains, and average grain size after different MDF passes.

### 3.1.3. Texture Evolution during High and Low Temperature Cycle Deformation

The EBSD inverse pole figure (IPF) maps of the high and low temperature cycle deformed samples are shown in Figure 10. The high angle grain boundaries (HAGBs, > 15°) and low angle grain boundaries (LAGBs, < 15°) are noted by black and white lines, respectively. No twins are observed because the deformation temperature is high enough to suppress the formation of the twins [23]. It is apparent that the 1MDFed sample exhibits a bimodal microstructure consisting of the fine DRXed grains with the grain size ranging from 0.53 to 9.95 μm and coarse unDRXed grains with the maximum grain size of 40.42 μm. Ref. [26] reports that that the average grain size of new grains formed by the PSN mechanism is smaller than the size of particles formed by other recrystallization mechanisms, which is consistent with the findings of this paper. The degree of DRX is improved with increasing the deformation passes except the 2nd pass and the fraction of DRXed grains increases from 59.0% of the 1MDFed sample to 98.4% of the 4MDFed sample, which can be considered to achieve complete DRX. Obviously, the deformation passes have a significant effect on the DRX behaviour.

Figure 11 illustrates the pole figure (PFs) of {0001} basal plane, including all grains, DRXed grains, and unDRXed grains. The maximum texture intensity of the 1MDFed sample is 35.279, as shown in Figure 11a–c, and it can be concluded that the texture orientation of the 1MDFed sample is mainly dependent on the unDRXed grains from Figure 10a–c. In addition, the unDRXed grains result in a typical basal texture. When the deformation pass reaches 2, the maximum texture intensity of the sample is 16.960, as shown in Figure 11d–f and the texture orientation is also attributed to the unDRXed grains from Figure 10d–f. The texture of 3MDFed and 4MDFed samples are attributed to the DRXed grains, and the maximum texture intensity of 3MDFed and 4MDFed samples are 14.269 and 8.184, respectively. It can be found that the basal texture becomes weaker with the increase of the deformation passes, and the DRXed grains play an important role on the texture orientation.

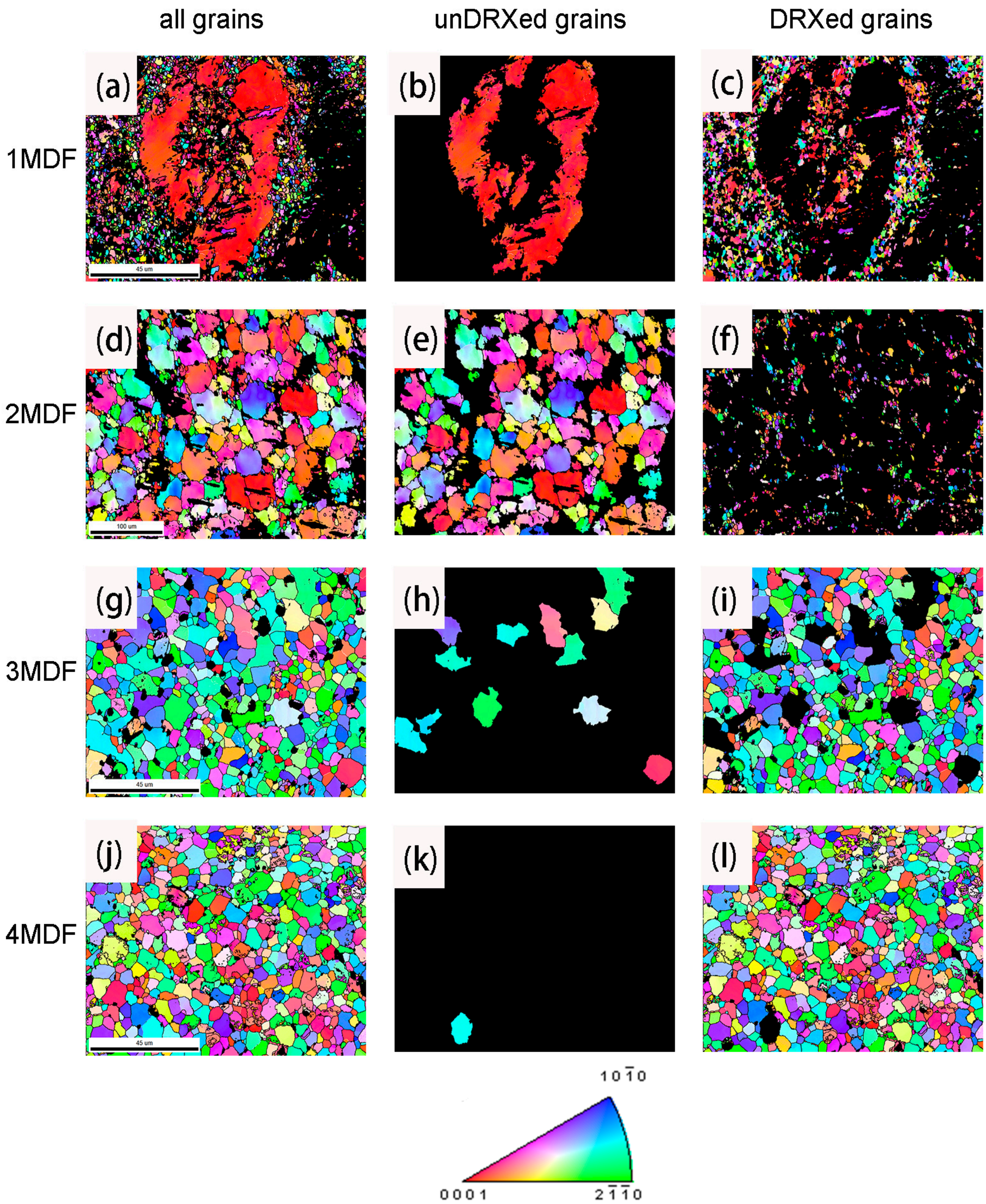


**Figure 10.** Inverse pole figure (IPF) maps for the experimental alloy after MDF to different passes, (**a**,**d**,**g**,**j**) the IPF images of all grains after different passes, (**b**,**e**,**h**,**k**) the IPF images of unDRXed grains after different passes, (**c**,**f**,**i**,**l**) the IPF images of DRXed grains after different passes, and the orientation triangle is also showed.

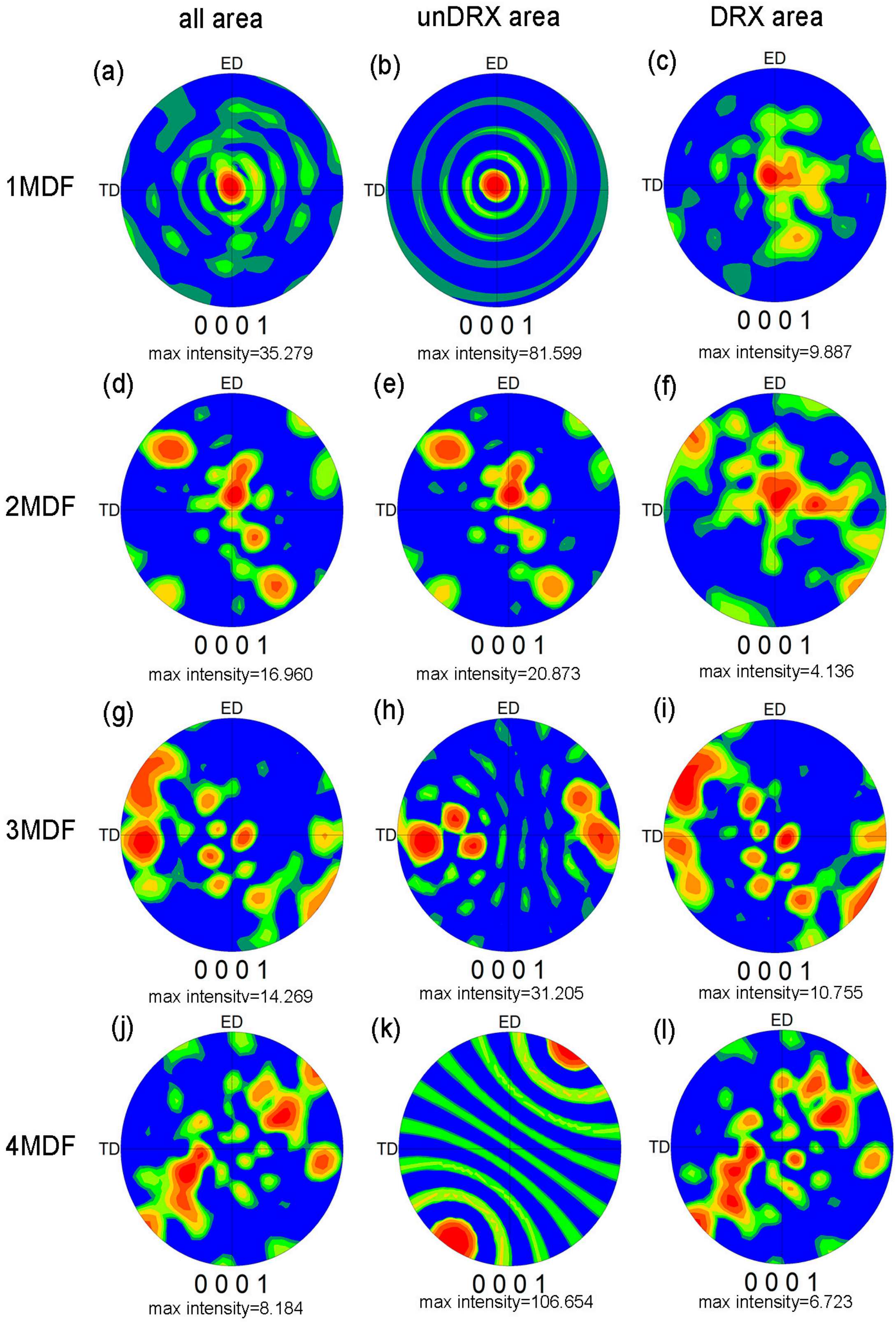


**Figure 11.** The {0001} pole figure (PF) of the specimens after MDF to different passes, (**a**,**d**,**g**,**j**) the {0001} pole figure (PF) of all area after different passes, (**b**,**e**,**h**,**k**) the {0001} pole figure (PF) of unDRX area after different passes, (**c**,**f**,**i**,**l**) ) the {0001} pole figure (PF) of all area after different passes, (**b**,**e**,**h**,**k**) the {0001} pole figure (PF) of DRX area after different passes.

### 3.2. Mechanical Performance and Fracture Behaviour

Figure 12 depicts the mechanical performance of the studied samples after different passes of high and low temperature cycle deformation by tensile tests at RT. The UTS, TYS, and FE of all the samples are exhibited. The UTS, TYS, and FE of the as-homogenized alloy after 520 °C (denoted as 0 pass) are 213 MPa, 182 MPa, and 3.2%, respectively. After 1 pass through the high and low temperature cycle deformation, the values of the UTS, TYS, and FE increase to 293 MPa, 257 MPa, and 8.4%, respectively, which are enhanced more than 37.6%. When the forging temperature is 46 °C, the UTS, TYS, and FE of the experimental sample dramatically decrease to 246 MPa, 227 MPa, and 7.60% due to the abnormal growth of the grains. When the deformation pass is up to 3 with the accumulative strain of 9, it is obvious to find that the UTS, TYS, and FE increase to 356 MPa, 264 MPa, and 11.5% rapidly. Further decreasing the temperature up to 420 °C, the sample exhibits the highest strength with the UTS of 405 MPa and TYS of 305 MPa, with a good elongation of 13.1%. It can be concluded that the increase of TYS is attributed to the fine grains during the tensile tests at RT. The refined grains lead to the increase of grain boundaries, which can be considered as grain boundary strengthening to improve the performance of GWZ alloy containing LPSO phases. At the same time, it is in line with the Hall-Petch equation:

$$\sigma_y = \sigma_0 + Kd^{-1/2}, \tag{2}$$

where $\sigma_y$ is the TYS, $\sigma_0$ and $K$ are material constants, and $d$ is the average grain size.

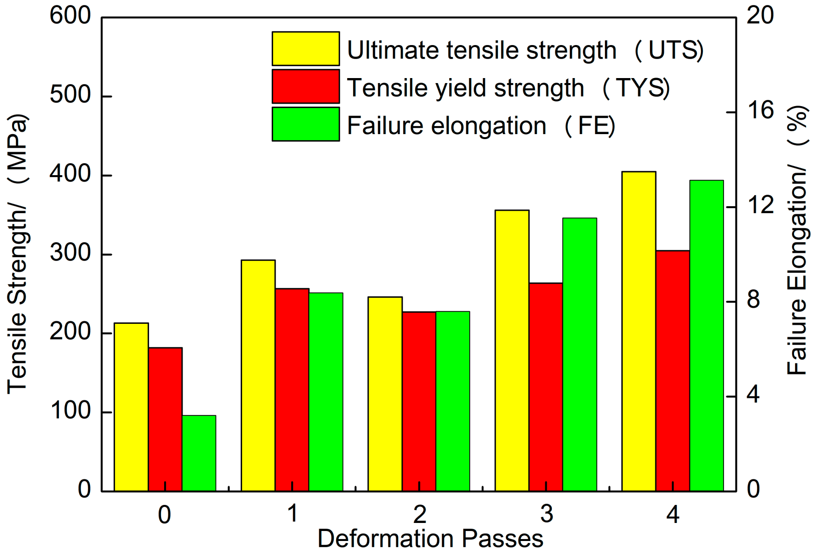


**Figure 12.** Tensile properties of the studied alloy after different deformation passes.

Figure 13 displays the tensile fracture morphologies of Mg-13Gd-4Y-2Zn-0.5Zr alloy after different passes. Mg alloys usually tend to fail brittle by cleavage fracture or quasi-cleavage fracture due to their restricted dislocation slip systems [27,28]. It can be found that massive cleavage planes and dimples are detected from the tensile fracture morphology, as shown in Figure 13, which can be demonstrated as brittle and ductile hybrid fracture mechanism. When the deformation pass is up to 2, it is obvious that there are amount cleavage planes and tear ridges that occur as shown in Figure 13b, which can be regarded as brittle fracture mechanism, causing the lowest UTS and TYS. Figure 13c,d show the amount of dimples in the fracture position after 3 and 4 passes on the condition of high and low cycle temperature, and they belong to the ductile fracture. However, the dimples that occur in the 4MDFed sample are more tiny compared with the 3MDFed sample, which lead to the highest YTS and TYS. In addition, the results indicate that the mechanical properties of the specimens after 4 passes through high and low temperature cycle deformation are also enhanced compared with the specimens after 4 passes on the condition of traditional decreasing temperature deformation (UTS:357

MPa, TYS:294 MPa). Thus, the high and low temperature cycle deformation is an effective method to improve the tensile properties of the studied alloy.

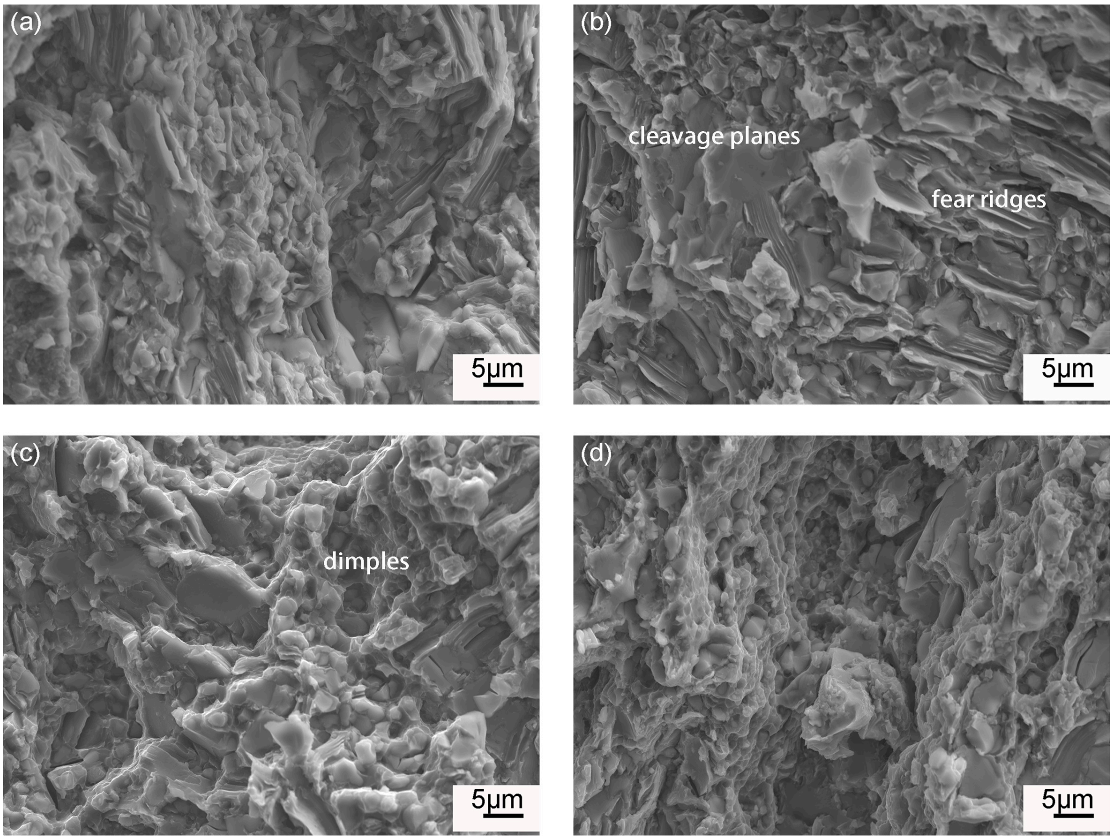


**Figure 13.** Tensile fracture morphologies of Mg-13Gd-4Y-2Zn-0.5Zr alloy after different passes: (**a**) 1 pass, (**b**) 2 passes, (**c**) 3 passes, (**d**) 4 passes.

## 4. Conclusions

The microstructure, texture evolution, and mechanical properties of the MDFed GWZ alloy containing LPSO phases on the condition of high and low temperature cycle deformation are experimentally investigated.

- The MDF method can lead to a refined microstructure with the average grain size of 5.20 μm, and a fully DRX (~98.4%) also can be achieved after 4 passes through high and low temperature cycle deformation.
- With the increase of deformation passes, the microstructure gradually changed from a bimodal microstructure to a uniform fine-grained microstructure. Deformation texture is transformed from a basal texture to random texture, and the maximum texture intensity gradually decreases.
- It is shown that the MDF method significantly improved mechanical properties of the experimental alloy, the excellent tensile properties are UTS of 405 MPa, TYS of 305 MPa, and FE of 13.14% after 4 passes.
- The grain refining mechanism is attributed to the increase of grain boundaries by PSN and DRX mechanism. The uniform microstructure is obtained mainly due to the SRX mechanism caused by the annealing treatment between deformation passes.
- The high and low temperature cycle deformation, as a new deformation method, can guide us to obtain a uniform and fine microstructure. Meanwhile, it also can be applied in industrial production.

**Author Contributions:** Conceptualization, B.D.; Methodology, Z.Z.; Software, X.C. and J.Z.; Validation, J.Y. and M.M.; Writing—original draft preparation, B.D.; Writing—review and editing, B.D., X.C., and J.Y. All authors have read and agreed to the published version of the manuscript.

**Funding:** This research was funded by the Shanxi Graduate Education Innovation Project, grant number 2019BY103, Key R&D program of Shanxi Province (International Cooperation), grant number 201903D421036, Scientific and Technological Innovation Programs of Higher Education Institutions in Shanxi, grant number 2018002.

**Conflicts of Interest:** The authors declare no conflict of interest.

## References

1. Mordike, B.L.; Ebert, T. Mg: Properties-applications-potential. *Mater. Sci. Eng. A* **2001**, *302*, 37–45. [CrossRef]
2. Mohamed, W.; Gollapudi, S.; Charit, I.; Murty, K.L. Formability of a wrought Mg alloy evaluated by impression testing. *Mater. Sci. Eng. A* **2018**, *712*, 140–145. [CrossRef]
3. Lu, J.W.; Yin, D.D.; Huang, G.H.; Quan, G.F.; Zeng, Y.; Zhou, H.; Wang, Q.D. Plastic anisotropy and deformation behavior of extruded Mg-Y sheets at elevated temperatures. *Mater. Sci. Eng. A* **2017**, *700*, 598–608. [CrossRef]
4. Fang, C.; Liu, G.; Liu, X.; Hao, H.; Zhang, X. Significant texture weakening of Mg-8Gd-5Y-2Zn alloy by Al addition. *Mater. Sci. Eng. A* **2017**, *701*, 314–318. [CrossRef]
5. Wu, Z.; Curtin, W.A. The origins of high hardening and low ductility in Mg. *Nature* **2015**, *526*, 62–67. [CrossRef]
6. Stanford, N.; Atwell, D.; Beer, A.; Davies, C.; Barnett, M.R. Effect of microalloying with rare-earth elements on the texture of extruded Mg-based alloys. *Scr. Mater.* **2008**, *59*, 772–775. [CrossRef]
7. Stanford, N. Micro-alloying Mg with Y, Ce, Gd and La for texture modification -a comparative study. *Mater. Sci. Eng. A* **2010**, *527*, 2669–2677. [CrossRef]
8. Bohlen, J.; Nürnberg, M.R.; Senn, J.W.; Letzig, D.; Agnew, S.R. The texture and anisotropy of Mg-zinc-rare earth alloy sheets. *Acta. Mater.* **2007**, *55*, 2101–2112. [CrossRef]
9. Mordike, B.L. Creep-resistant Mg alloys. *Mater. Sci. Eng. A* **2002**, *324*, 103–112. [CrossRef]
10. Rokhlin, L.L. *Mg Alloys Containing Rare Earth Metals: Structure and Properties*; Taylor & Francis Ltd.: London, UK; New York, NY, USA, 2003; pp. 1–256.
11. Homma, T.; Knito, N.; Kamado, S. Fabrication of extraordinary high-strength Mg alloy by hot extrusion. *Scr. Mater.* **2009**, *61*, 644–647. [CrossRef]
12. He, S.M.; Zeng, X.Q.; Peng, L.M.; Gao, X.; Nie, J.F.; Ding, W.J. Microstructure and strengthening mechanism of high strength Mg-10Gd-2Y-0.5Zr alloy. *JALLC* **2007**, *427*, 316–323. [CrossRef]
13. Yamasaki, M.; Anan, T.; Yoshimoto, S.; Kawamura, Y. Mechanical properties of warm-extruded Mg-Zn-Gd alloy with coherent 14H long periodic stacking ordered structure precipitate. *Scr. Mater.* **2005**, *53*, 799–803. [CrossRef]
14. Yu, Z.J.; Xu, C.; Meng, J.; Zhang, X.H.; Kamado, S. Effects of pre-annealing on microstructure and mechanical properties of as-extruded Mg-Gd-Y-Zn-Zr alloy. *J. Alloys Compd.* **2017**, *729*, 627–637. [CrossRef]
15. Peng, Q.M.; Hou, X.L.; Wang, L.D.; Wu, Y.M.; Cao, Z.Y.; Wang, L.M. Microstructure and mechanical properties of high performance Mg-Gd based alloys. *Mater. Des.* **2009**, *30*, 92–296. [CrossRef]
16. Nie, K.B.; Deng, K.K.; Wang, X.J.; Xu, F.J.; Wu, K.; Zheng, M.Y. Multidirectional forging of AZ91 Mg alloy and its effects on microstructures and mechanical properties. *Mater. Sci. Eng. A* **2015**, *624*, 157–168. [CrossRef]
17. Huang, H.; Zhang, J. Microstructure and mechanical properties of AZ31 Mg alloy processed by multi-directional forging at different temperatures. *Mater. Sci. Eng. A* **2016**, *674*, 52–58. [CrossRef]
18. Saboori, A.; Dadkhah, M.; Pavese, M.; Manfredi, D.; Biamino, S.; Fino, P. Hot deformation behaviour of Zr-1%Nb alloy: Flow curve analysis and microstructure observations. *Mater. Sci. Eng. A* **2017**, *696*, 366–373. [CrossRef]
19. Yu, Z.J.; Huang, Y.D.; Mendis, C.L.; Hort, N.; Meng, J. Microstructural evolution and mechanical properties of Mg-11Gd-4.5Y-1nD-1.5Zn-0.5Zr alloy prepared via pre-ageing and hot extrusion. *Mater. Sci. Eng. A* **2015**, *624*, 23–31. [CrossRef]
20. Yu, Z.J.; Huang, Y.D.; Gan, W.M.; Zhong, Z.Y.; Hort, N.; Meng, J. Effects of extrusion ratio and annealing treatment on the mechanical properties and microstructure of a Mg-11Gd-4.5Y-1Nd-1.5Zn-0.5Zr (wt%) alloy. *J. Mater. Sci.* **2017**, *52*, 6670–6686. [CrossRef]

21. Xia, X.; Chen, Q.; Zhao, Z.; Ma, M.; Li, X.; Zhang, K. Microstructure, texture and mechanical properties of coarse-grained Mg-Gd-Y-Nd-Zr alloy processed multidirectional forging. *J. Alloys Compd.* **2015**, *638*, 67–276. [CrossRef]
22. Asqardoust, S.; Zarei-Hanzaki, A.; Abedi, H.R.; Krajnak, T.; Minarik, P. Enhancing the strength and ductility in accumulative back extruded WE43 Mg alloy through achieving bimodal grain size distribution and texture weakening. *Mater. Sci. Eng. A* **2017**, *698*, 218–229. [CrossRef]
23. Xiao, H.; Tang, B.; Liu, C.; Gao, Y.; Yu, S.; Jiang, S. Dynamic precipitation in a Mg-Gd-Y-Zr alloy during hot compression. *Mater. Sci. Eng. A* **2015**, *645*, 241–247. [CrossRef]
24. Ramezani, S.M.; Zarei-Hanzaki, A.; Abedi, H.R.; Salandari-Rabori, A.; Minarik, P. Achievement of fine-grained bimodal microstructures and superior mechanical properties in a multi-axially forged GWZ Mg alloy containing LPSO structures. *J. Alloys Compd.* **2019**, *793*, 134–145. [CrossRef]
25. Salandari-Rabori, A.; Zarei-Hanzaki, A.; Fatemi, S.M.; Ghambari, M.; Moghaddam, M. Microstructure and superior mechanical properties of a multi-axially forged WE Mg alloy. *J. Alloys Compd.* **2017**, *693*, 406–413. [CrossRef]
26. Asqardoust, S.; Zarei-Hanzaki, A.; Fatemi, S.M.; Moradjoy-Hamedani, M. High temperature deformation behaviour and microstructural evolutions of a high Zr containing WE Mg alloy. *J. Alloys Compd.* **2016**, *669*, 108–116. [CrossRef]
27. Nie, K.B.; Wang, X.J.; Deng, K.K.; Xu, F.J.; Wu, K.; Zheng, M.Y. Microstructures and mechanical properties of AZ91 Mg alloy processed by multidirectional forging under decreasing temperature. *J. Alloys Compd.* **2014**, *617*, 979–987. [CrossRef]
28. Li, Z.F.; Dong, J.; Zeng, X.Q.; Lu, C.; Ding, W.J. Influence of Mg17Al12 intermetallic compounds on the hot extruded microstructures and mechanical properties of Mg-9Al-1Zn alloy. *Mater. Sci. Eng. A* **2007**, *466*, 134–139. [CrossRef]